풍화암에 근입된 현장타설 말뚝의 하중 전이 특성
Shear Load Transfer Characteristics of Drilled Shafts in Weathered Rocks

정상섬[1], Sang-Seom Jeong, 조성한[2], Sung-Han Cho, 김수일[3], Soo-Il Kim

[1] 연세대학교 공과대학 토목공학과 부교수, Associate Professor, Department of Civil Eng., Yonsei Univ.
[2] LG건설 토질 및 기초팀 과장, Project Engineer, Geotechnical Department, LG Construction Co., Ltd.
[3] 연세대학교 공과대학 토목공학과 교수, Professor, Department of Civil Eng., Yonsei Univ.

SYNOPSIS : The load distribution and deformation of drilled shafts subjected to axial loads were evaluated by a load transfer approach. The emphasis was on quantifying the load transfer mechanism at the interface between the shafts and surrounding highly weathered rocks based on a numerical analysis and small-scale tension load tests performed on nine instrumented piles. An analytical method that takes into account the soil coupling effect was developed using a modified Mindlin's point load solution. Based on the analysis, a single-modified hyperbolic model is proposed for the shear transfer function of drilled shafts in highly weathered rocks. Through comparisons with field case studies, it is found that the prediction by the present approach is in good agreement with the general trend observed by in-situ measurements.

Key words : shear load-transfer, drilled shaft, weathered rock, tension load test, soil coupling, single-modified hyperbolic model, in-situ measurements

1. INTRODUCTION

In Korea, a number of huge construction projects such as land reclamation projects for an international airport, high-speed railways, and many harbor constructions are in progress in urban and coastal areas. Drilled shafts are frequently used in those areas as a viable replacement for driven piles for two applications: deep water offshore foundations and foundations in urban areas where the noise and vibration are associated with pile driving. Over 90% of the drilled shafts constructed in Korea are embedded in weathered rocks. The weathered rocks, which occupy two-thirds of the total land area of the Korean peninsula, are generally the results of the physical weathering of granite-gneiss of varying thicknesses ranging up to 40 meters.

Two general considerations are important in the construction and design of drilled shafts in rocks: selection and implementation of construction details and consideration of load transfer in skin friction and in endbearing in making a design. A comprehensive study of drilled shafts has been reported by Reese and O'Neill (1988). They report that the

magnitude and distribution of the side resistance transferred down to the tip are highly influenced by the compressive strength of rock and the settlement between the drilled shaft and the rock. This is based on the concept that both side resistance and endbearing will not develop simultaneously and thus detailed studies, including field test, are needed in many instances to confirm a design.

A large number of load tests on instrumented drilled shafts have been performed to understand the load transfer mechanisms (Reese and O'Neill 1988). Presently, it is generally accepted that the ultimate shaft resistance for large bored piles is mobilized after small displacements of the shaft with respect to the surrounding soil. On the other hand, the ultimate value of point resistance is only reached at very large relative displacements of the pile tip(De Beer 1986; Reese and O'Neill 1988; Ghionna et al. 1993; Fioravante et al. 1994). In this respect, the evaluation of the overall ultimate load capacity of a drilled shaft is of minor relevance for design purposes because long before the ultimate capacity is attained, a settlement is reached that may cause the collapse of the supported structure. Therefore, the design of a drilled shaft should be made with regard to the two limiting states, the ultimate limit and serviceability limit (Ghionna et al. 1994; Reese and O'Neill 1988).

Since 1970, much work has been done in the area of soil-structure interaction of drilled shaft in clay (Engeling et al. 1974; O'Neill et al. 1970), hard rock sockets (Webb 1977) and soft rocks such as shale or clay-shale (Goeke and Hustad 1979). However, less is known about the behavior of drilled shafts in weathered rocks of granite-gneiss. The theoretical concepts presented in this paper were developed to provide a basis for a load transfer criterion that would be applicable to drilled shafts installed in highly weathered rocks of granite-gneiss. The validity of the criterion was tested against field case studies.

2. METHODS AVAILABLE FOR PILE LOAD TRANSFER

The load transfer from the pile to soil must be considered in order to achieve structural compatibility between loads and deformation. Basically, there are two analytical methods to calculate the load-deformation behavior of axially loaded piles.

2.1 Load Transfer Curve Methods

According to these methods (Coyle and Reese 1966; Vijayvergiya 1977; Kraft et al. 1981; Baquelin et al. 1982; Castelli et al. 1992; O'Neill and Hassan 1994), the load-deformation relationship for drilled shafts is calculated on the basis of load transfer curve utilizing subgrade reactions. The soil is represented by a set of load-transfer curves representing the soil resistance as a function of pile displacements at several discrete points along the pile including the point. Finite difference techniques are often used to solve the differential equations governing the compatibility between the pile displacement and the load transfer along a pile and between the displacement and the resistance at the tip of the pile assuming that the load transfer at a certain pile section and the pile tip resistance are independent of pile displacement elsewhere. These techniques are generally based on load tests on full-scale, instrumented shafts and parametric finite element analyses of pile-soil interactions which are represented by unit shear load transfer vs. local shaft displacement relations (f-w curves). Therefore, the definition of the f-w relations is the key to the successful understanding to a real pile-soil response. There are several techniques available for predicting the f-w curves in soils (Vijayvergiya 1977; Kraft et al. 1981; Castelli et al. 1992) and rocks (Baquelin et al. 1982; O'Neill and Hassan 1994). All these methods model the f-w curves by elastic-plastic models where the ultimate value f_{max} is obtained in the same way as it would be for shaft friction in pile capacity computations.

2.2 Elastic Methods

The elastic methods based on the theory of elasticity have been suggested by Poulos and Davis (1968), Mattes and Poulos (1969), Kuwabara and Poulos (1989) and Chow (1990). This method has been used to investigate the pile-soil system which is analyzed as a continuous elastic or elastoplastic medium using either modified Mindlin's solution or a finite element formulation. In the method using Mindlin's equation, the response of rigid or compressible piles embedded in a homogeneous isotropic linear elastic medium is computed by a rigorous analysis based on superimposing the influence of the load transfer along the pile and the pile point resistance at a certain point. This is an oversimplification of the soil response. However, this method has the advantage of taking into account the stress distribution within the soil.

3. LOAD TRANSFER ANALYSIS BY COUPLED SOIL RESISTANCE

3.1 Method of Analysis

In the normal load transfer mechanism, the stress at and displacement of each point along a pile are influenced by the stress at other points; the degree of influence decreases with an increase in distance from the point of interest. The subgrade-reaction approach assumes that the displacement at any point depends only on the stress at that point. Soil-pile interaction is represented by springs that relate shear stress on the soil-pile interface and displacement of the pile. Thus, the continuity of the soil mass is not properly taken into account.

The load transfer method used in this study, however, considers the continuity of the soil mass by applying Mindlin's solution (Poulos and Davis 1968). Here, the pile point displacement caused by the load carried by the pile shaft can be expressed as:

$$s_2 = \frac{D}{E_s} \sum_{j=1}^{n} (I_{bj} f_j) \tag{1}$$

where, f_j = shear transfer function on element j, I_{bj} = vertical displacement factor for the base due to shear stress on element j (Fig. 1):

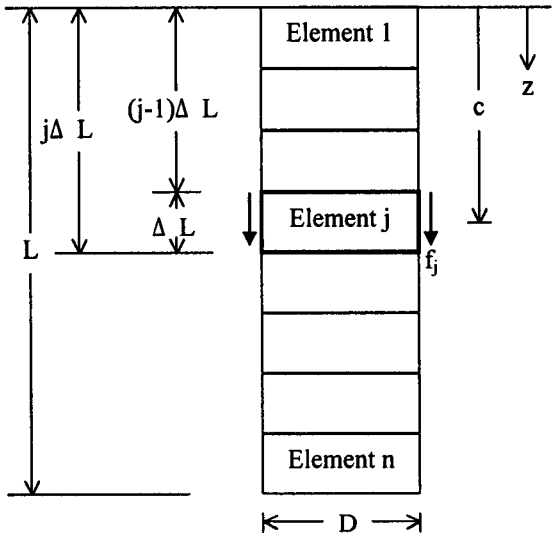

FIG. 1. Geometry of a Pile (After Poulos and Davis 1968)

$$I_{bj} = \pi \int_{(j-1)\Delta L}^{j\Delta L} I_p dc \tag{2}$$

where the length of the element, $\Delta L = L/n$, c= embedded depth to element j, and I_p = influence factor for vertical displacement due to a vertical point load. According to Mindlin's equation, I_p is given by:

$$I_p = \frac{(1+\nu_s)}{8\pi(1-\nu_s)}\left\{\frac{z_1^2}{R_1^3} + \frac{(3-4\nu_s)}{R_1} + \frac{(5-12\nu_s+8\nu_s^2)}{R} + \frac{(3-4\nu_s)z^2 - 2cz + 2c^2}{R^3} + \frac{6cz^2(z-c)}{R^5}\right\} \tag{3}$$

where ν_s = Poisson's ratio, $z = h + c$, $z_1 = h - c$, $R^2 = z^2 + D^2/4$, and $R_1^2 = z_1^2 + D^2/4$.

The integral with respect to c in equation (2) can be evaluated analytically and expressed as:

$$I_{bj} = \frac{(1+\nu_s)}{8(1-\nu_s)}\left\{\frac{z_1}{R_1} - 4(1-\nu_s)\ln(z_1 + R_1) + 8(1-2\nu_s+\nu_s^2)\ln(z+R) + \frac{2h^2 z/r^2 - 4h - (3-4\nu_s)z}{R} + \frac{2(hr^2 - h^2z^3/r^2)}{R^3}\right\} \tag{4}$$

where, h = embedded depth, and r = pile radius. By the substitution of equation (4) into equation (1), the pile point displacement (s_2) caused by the load carried by the pile shaft can be calculated.

3.2 Solution Procedure

In this paper, a model to compute loads and deformations of drilled shafts subjected to axial load based on the transfer function approach is derived. Simple numerical solution procedures are developed for fairly general conditions (non-linear stress-strain behavior at the pile-soil interface and non-homogeneous soil conditions).

The equilibrium of an elastic pile element along its axis can be written as:

$$\frac{d^2 w_z}{dz^2} = \frac{f_z C_p}{E_p A_p} \tag{5}$$

where w_z is the vertical displacement of the pile shaft, E_p, C_p, A_p are the modulus of elasticity, the perimeter and cross-sectional area of the pile, respectively, and f_z is the unit shear transfer function exerted by the soil. For general transfer functions, a numerical solution procedure is needed. A finite difference approximation of equation (5) can be written as:

$$\frac{1}{(\Delta L)^2}(w_{i-1} - 2w_i + w_{i+1}) = \frac{C_p}{E_p A_p} f_i \tag{6}$$

For an initially applied external load, Q_1, the following condition at i point is:

$$Q_i = Q_1 - \sum_{j=1}^{i-1} f_j L_j C_p \tag{7}$$

It has been found that a convenient and powerful procedure for solving the problem for non-homogeneous soil profiles and complicated inelastic transfer functions is to formulate a full set of non-linear equations by applying equations (1)-(7). The nonlinear analyses were done to take into account the soil coupling effect at the pile-soil interface

and used an iterative and incremental analysis. For an elastoplastic state, the material stiffness was continually changed and thus the iterative process was repeated until the changes in the material stiffness between successive iterations were negligible. The incremental procedure was composed of dividing the external load into many small and equal increments which were applied incrementally.

4. TENSION LOAD TEST

Field tests were conducted at the Seohae grand bridge site in Korea. A thin layer of highly weathered silty sand overlies the Pyeongtaeg Formation of Cambrian Age. The Pyeongtaeg Formation, which represents the uppermost bedrock material, is composed primarily of soft granite-gneiss rock. The subsurface investigation was performed on nine boring holes and NX-size core samples on triple core barrel were recovered up to 100% from the uppermost bedrock. Visual inspection of the bedrock samples indicated that the sample in the triple core barrel was difficult to core without fracture and was classified into highly weathered rocks based on weathering grades (Lee and de Freitas, 1989). The roughness of rock samples were recognizable to two different types: rough surface with high quartz grains and relatively smooth surface with small amount of quartz grains compared to the former one.

To investigate the shear transfer curves of drilled shafts placed in soft granite-gneiss rocks, small-scale tension load tests were performed on nine instrumented piles. A schematic representation of an instrumented drilled shaft subjected to a loading test is shown in Fig. 2. The holes of 165 mm in diameter and 6000 mm in depth were drilled by wash and rotary techniques. The steel bar was then inserted into the hole and anchored with cement grout (water/cement ratio of 0.5). A hollow 700 kN hydraulic jack was used to apply loads to the piles. The applied load and displacement were measured using a hollow load cell and telltale installed at the pile top and the pile point, respectively. All tests were conducted 28 days after the grouting of the piles when the grout had developed a compressive strength and modulus of elasticity of 2.8×10^4 kN/m^2 and 3.5×10^7 kN/m^2, respectively. For the tension load test, a constant load was applied to the pile and sustained for 15 minutes at each load level. This procedure was repeated until the anticipated design load was reached and total of eight load increments was applied.

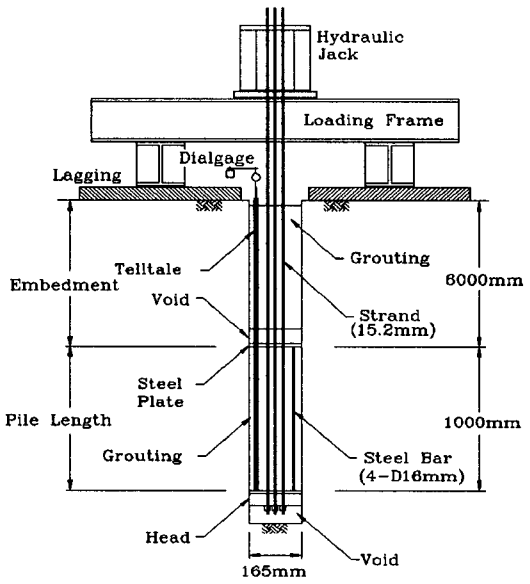

FIG. 2.Tension Load Test Details

5. TEST RESULTS AND DISCUSSION

The relationship between load transfer and shaft displacement for a short increment along the shaft can be generated by plotting, for each test load, the average load transfer over the increment versus the average displacement of the increment. The shaft unit resistance- displacement curves for 9 test piles were generated according to the above procedures as shown in Fig. 3.

As shown in Fig. 3, shear transfer curves can be categorized typically into two different types. Shaft 1 groups composed of 5 test piles and shaft 2 groups composed of 4 test piles were embedded in highly weathered rocks with rough- and smooth-interface, respectively, produced by wash and rotary drilling. At the end of the testing period, two piles were excavated and shaft roughness examined. Two piles composed of Shaft 1 groups and Shaft 2 groups in which small, triangular asperities were produced naturally were found to have approximately 5 mm and 1.5 mm in depth of asperity, respectively. Based on the study presented by Horvath et al. (1983), roughness effects for test piles were examined by a roughness factor (RF) to check the borehole roughness. The range of RF is 0.01-0.03 (Horvath et al., 1983), which can be assumed to represent a smooth shaft. Though total length of the path from the top of the socket to the base, including the path along natural asperities, was not measured for test piles, RF for the test shafts is: the average value of RF on shaft 1 groups is about 0.1, representing rough shaft and the corresponding value of shaft 2 groups is about 0.02, representing smooth shaft.

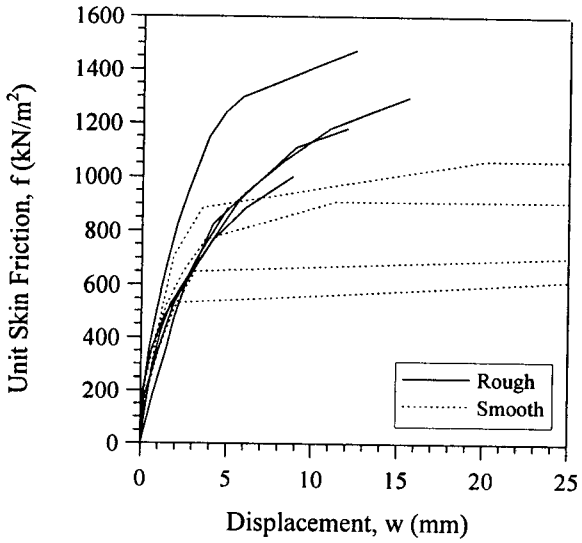

FIG. 3.Unit Skin Resistance-Displacement Curves

For the rough surface shaft (solid line), shaft resistance increased sharply within 2mm displacement, beyond which it continued to increase rapidly toward the failure state as displacement increased. On the other hand, the corresponding curve for the smooth surface shaft (dotted line) shows an initial sharp increase of side resistance and then followed with a more gradual increase, until a constant resistance was reached at about 5 mm displacement. The reason for this behavioral difference between rough surface and smooth surface is explained by the fact that the rough interface will produce more shearing resistance than the smooth interface. Therefore the slope of the f-w curve after reaching 5 mm displacement is that failure of the adhesive bond and simultaneous shearing of asperities along an element of shaft result in a constant frictional resistance for the smooth interface and frictional and dilatant natures for the rough interface, respectively. Therefore, This trend is in general agreement with the observations of O'Neill and Hassan (1994) and

Townsend et al. (1993).

The typical load transfer characteristics of rough interface shaft based on pile load tests and predictions using Castelli et al. (1992), O'Neill and Hassan (1994), Vijayvergiya (1977), and Baquelin et al. (1982) transfer functions are plotted on the same graph as in Fig. 4. The material properties determined by a pressuremeter test for prediction purposes were: the granite-gneiss rock Young's modulus, E_s = 300000 kN/m^2, Poisson's ratio, ν = 0.3. The results by load tests are in good agreement with the Castelli, O'Neill and Hassan models, compared with the predictions by the Vijayvergiya and Baquelin models. The reason for this behavioral difference is that w_{max} in Vijayvergiya model is assumed as an unique value of 5mm and the f-w curve by Baquelin model is a bi-linear function whereas the results by load tests show the continuous nonlinear increment of shaft resistance toward the f_{max} as displacement increased. Therefore, the following shear transfer curve using a hyperbolic load transfer function can be introduced:

$$f = \frac{w}{\frac{1}{S_i} + \frac{w}{f_{max}}} \tag{8}$$

where, f = unit skin resistance mobilized along a pile segment at a movement, w, S_i = initial tangent of the load transfer function and f_{max} = maximum unit skin resistance.

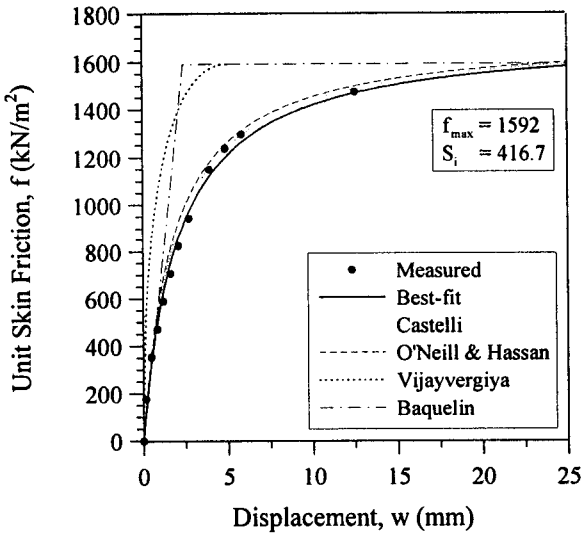

FIG. 4. Shear Load-Transfer Curves on Test Pile 1 (Rough Surface)

On the other hand, the corresponding curve for the smooth interface shaft is plotted on the same graph as in Fig. 5. The material properties used for Young's modulus and Poisson's ratio were the same values as those of rough interface. The results by load tests are in good agreement with the Vijayvergiya model, compared to the predictions by the O'Neill and Hassan and Baquelin model. The reason for this behavioral difference is that the f-w curve by O'Neill and Hassan model can be applied to the regular asperity patterns for irregular interface and in Baquelin model, the elastic part (first slope) of the f-w curve is linear whereas the results by load tests show an initial sharp increase of side resistance and then followed with a more nonlinear increase until a constant resistance. Though the prediction by Vijayvergiya's f-w function simulates well the general trend observed for the smooth interface shaft, it was derived based on an assumption that w_{max} is recommended to a specified value without considering soil stiffness with varying depth and thus it is not appropriate to evaluate the soil parameters properly. Therefore in this case, the following shear transfer curve using a modified hyperbolic load transfer function can be introduced:

$$f = \frac{w}{\frac{1}{S_i} + \frac{w}{\alpha_1 f_{max}}} \tag{9}$$

where, α_1 = curve-fitting constant larger than 1.0.

In the modified hyperbolic transfer function, f approaches its maximum value $\alpha_1 f_{max}$ until a ultimate resistance f_{max} is reached, beyond which it is modeled as perfectly plastic. This transfer function is quite similar to the hyperbolic model with the value α_1=1.0 whereas for α_1 larger than 1.0, the curve shape is kind of elastic-perfectly plastic. Thus, regardless of the surface roughness, the transfer function can be represented by modified hyperbolic transfer function by adjusting the α_1 value properly.

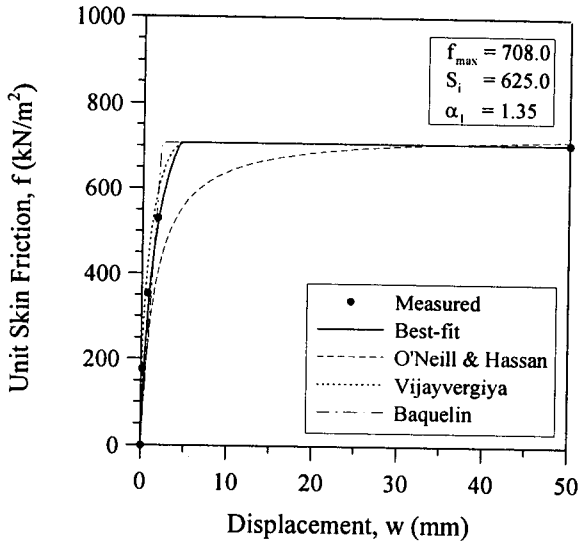

FIG. 5. Shear Load-Transfer Curves on Test Pile 7 (Smooth Surface)

6. PARAMETRIC STUDY

The above transfer function, f, is a direct function of the pile displacement, w, initial tangent modulus, S_i, maximum unit skin resistance, f_{max} and a curve-fitting constant, α_1. In most of the proposed models(O'Neill and Hassan 1994; Baquelin et al. 1982), the initial tangent modulus of the load transfer function, S_i is taken proportional to Young's modulus, E_s, and is opposed to the diameter of the pile. The modified hyperbolic model proposed by the form of equation(9) is based on the small-scale tension load tests and thus, in conflict with the known behavior of full-scale drilled shafts. A major parameter influencing the shear load transfer function is the initial tangent modulus, S_i. To obtain detailed information on the behavior of the shear transfer, a series of numerical analyses on S_i were performed for different pile diameters and soil conditions.

The response of a drilled shaft was analyzed by using a two-dimensional nonlinear finite element approach. The two-dimensional model includes standard axisymmetric finite element techniques. The Finite element mesh for a typical case is shown in Fig. 6. The mesh consists of two-dimensional 15-noded solid triangular elements and was assumed to be resting on a rigid layer, and the vertical boundaries at the left- and right-hand sides were assumed to be on rollers to allow downward movement of weathered rock layers due to external surcharge loading. The pile element was assumed to remain elastic at all times, while the surrounding rock was idealized as a Mohr-Coulomb elastoplastic material. The interface element was comprised of one-dimensional quadratic 5-node elements, each element a one five-node surface compatible with the adjacent solid elements; the two surfaces coincide initially. This model was selected in the element

library of PLAXIS (version 6.1 from Plaxis BV, Inc., Netherlands), the commercial finite element package used for this work. The meshes with various degrees of refinement, especially in the region surrounding the piles and near the pile head and tip where singularities occur, were tested until satisfactory convergence of the rock stresses around the pile was reached.

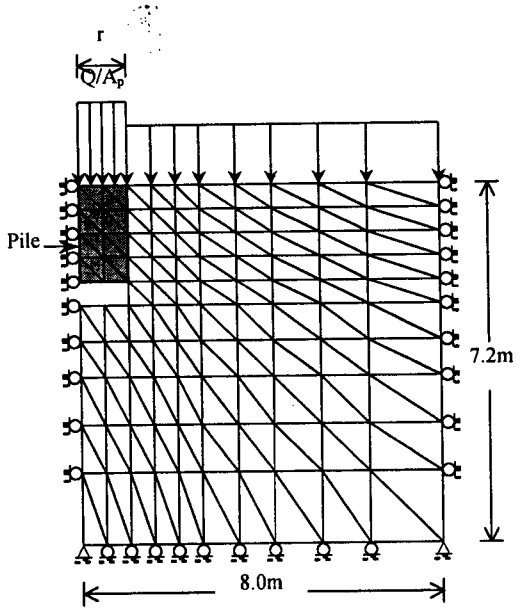

FIG. 6. Element Mesh and Boundary Condition

It was assumed that the external load was applied to the pile top and ground surface of the rock as a distributed load. The water table was estimated constant at the ground surface and a drained analysis was performed. The shaft friction was calculated on the basis of the effective stress parameters. The material properties chosen to represent a weathered rock were selected accordingly; the required data were back calculated by fitting the measured axial forces in a 165mm tension pile load test to that computed by the finite element method. Table 1 shows the material properties and geometries used in this study. The elastoplastic analyses were run to take into account the local yielding at the pile-rock interface and used an iterative and incremental analysis. Factors which are relevant to the shaft resistance will be discussed in detail.

Table 1. Material Properties and Geometries

Surface Roughness		Rough	Smooth
Soil Properties	Internal Friction Angle ϕ' (°)	38	32
	Cohesion, c' (kN/m^2)	300	600
	Dilation Angle, ψ (°)	2	0
	Elastic Modulus, E_s (kN/m^2)	100000, 300000, 600000, 900000, 1200000, 1500000, 1800000, 2000000	
	Poisson's Ratio, v	0.30	
	Unit Weight, γ (kN/m^3)	21.0	
Pile Properties	Elastic Modulus, E_s (kN/m^2)	35000000	
	Poisson's Ratio, v	0.17	
	Length, L (m)	1.0	
	Diameter, D (mm)	165, 300, 600, 900, 1200, 1500	

6.1 Influence of Surcharge Loading

Fig. 7 shows the shaft friction resistance as a function of various surcharge loadings for the two surface roughnesses. This figure shows that there was little difference in friction resistance with an increase of surcharge loading from 63 to 315 kN/m^2. It is shown that the initial tangent modulus, S_i is almost constant, irrespective of different surcharge loadings. Therefore, the surcharge loading for prediction purposes thereafter was taken to be, in all cases, the same as 126 kN/m^2 of the surcharge loading applied in the tension load test.

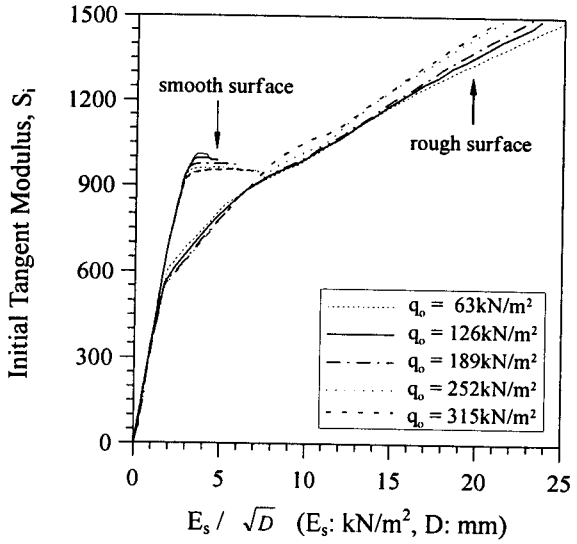

FIG. 7. Inflence of Surcharge Load in Shaft Resistance

6.2 Effect of Young's Modulus and Shaft Diameter (E_s/D)

Fig. 8 shows the effect of Young's modulus of soil and pile diameter on the unit skin resistance. As the E_s / D increases, the average shear stress along the pile shaft and initial tangent modulus tend to increase. This trend is also in good agreement with the proposed models(O'Neill and Hassan, 1994; Baquelin et al. 1982). However, the fitness of the initial tangent modulus is more closely related to $E_s / \sqrt{D}$ than to E_s / D as shown in Fig. 8. Thus, commonly used methods for calculating initial tangent modulus by using the results of E_s / D values can substantially underestimate the degree of initial slope in realistic situations.

7. PROPOSED LOAD TRANSFER FUNCTION

The information obtained by the two-dimensional parametric analysis can play a significant role in determining the initial tangent modulus. It is shown that the initial tangent modulus of the load transfer function, S_i, is proportional to Young's modulus, E_s, and inversely proportional to $\sqrt{D}$, based on a numerical analysis. Therefore a well defined testing program is frequently necessary in order to obtain very good estimates of the E_s of rock since the Young's modulus of rock is highly dependent on the strain level and testing methods. In these respects, by considering proposed uniaxial compressive strength (q_u) vs. E_s relations (Deere, 1968, and Peck, 1976, Horvath and Kenney, 1979), a simple method is proposed for computing the S_i for rock with q_u instead of adopting E_s directly.

Goodman (1980) studied the problem of socketing a concrete pier into rock and suggested the following equation.

$$f_{max} = 0.05 q_u \tag{10}$$

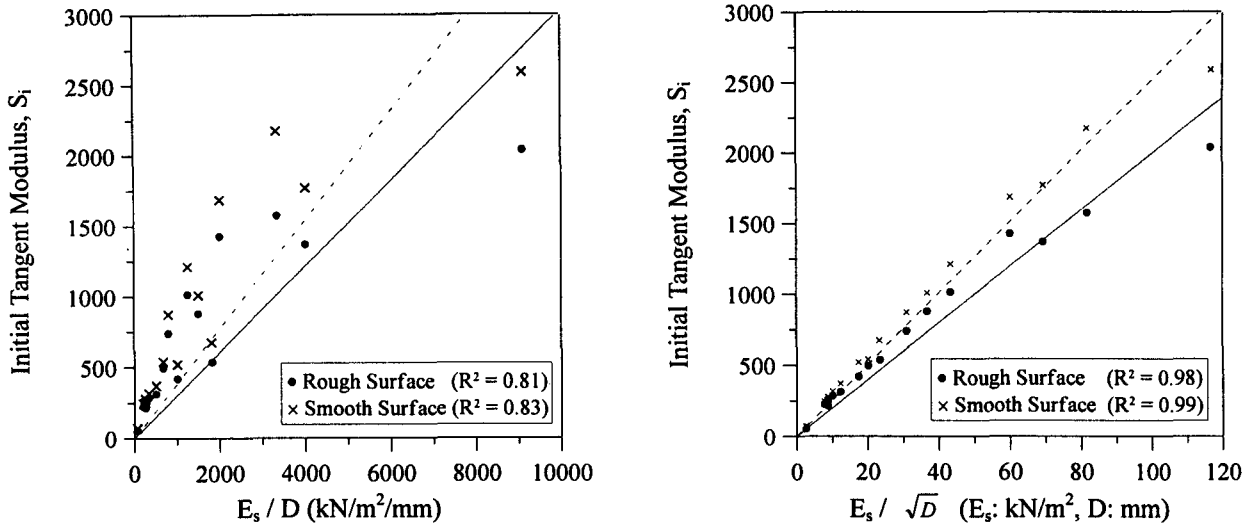

FIG. 8. Comparison of Initial Tangent Modulus (Linear Regression Analysis):
(a) Influence of E_s / D; (b) Influence of $E_s / \sqrt{D}$

As a result, by introducing equation (10), the generalized function, S_i is expressed as

$$S_i = \frac{CE_s}{\sqrt{D}} = \frac{C\alpha_1 f_{max}}{\sqrt{D}} \tag{11}$$

where, C = proportional constant, α_1 = curve-fitting constant, and D = pile diameter.

The corresponding shear transfer function of equation (9) for the drilled shafts is:

$$f = \frac{w}{\frac{\sqrt{D}}{C\alpha_1 f_{max}} + \frac{w}{\alpha_1 f_{max}}} \tag{12}$$

This is the proposed single modified hyperbolic function. Next, for the purpose of applying the transfer function of equation (12), C and α_1 are evaluated as follows:

Normalized in terms of f_{max}, equation (12) will be

$$\frac{f}{f_{max}} = \frac{w}{\frac{\sqrt{D}}{C\alpha_1} + \frac{w}{\alpha_1}} \tag{13}$$

In order to evaluate the C factor and curve fitting constant, α_1, in equation (13), it is required to transform the coordinates (w,f) into (w, w/(f/f_{max})) and therefore, equation (13) will be a linear line with a slope of $1/\alpha_1$ and a intercept of $\sqrt{D}/(C\ \alpha_1)$ as follows:

$$\frac{w}{f / f_{max}} = \frac{\sqrt{D}}{C\alpha_1} + \frac{w}{\alpha_1} \tag{14}$$

Fig. 9 shows the shear load transfer curves in transformed coordinates (equation 14) based on the results obtained in tension load tests. From the linear regression analysis, rough-and smooth-interface shaft will be the following linear transfer lines, respectively.

$$\frac{w}{f / f_{max}} = 3.33 + w \tag{15}$$

$$\frac{w}{f / f_{max}} = 1.52 + \frac{w}{1.35} \tag{16}$$

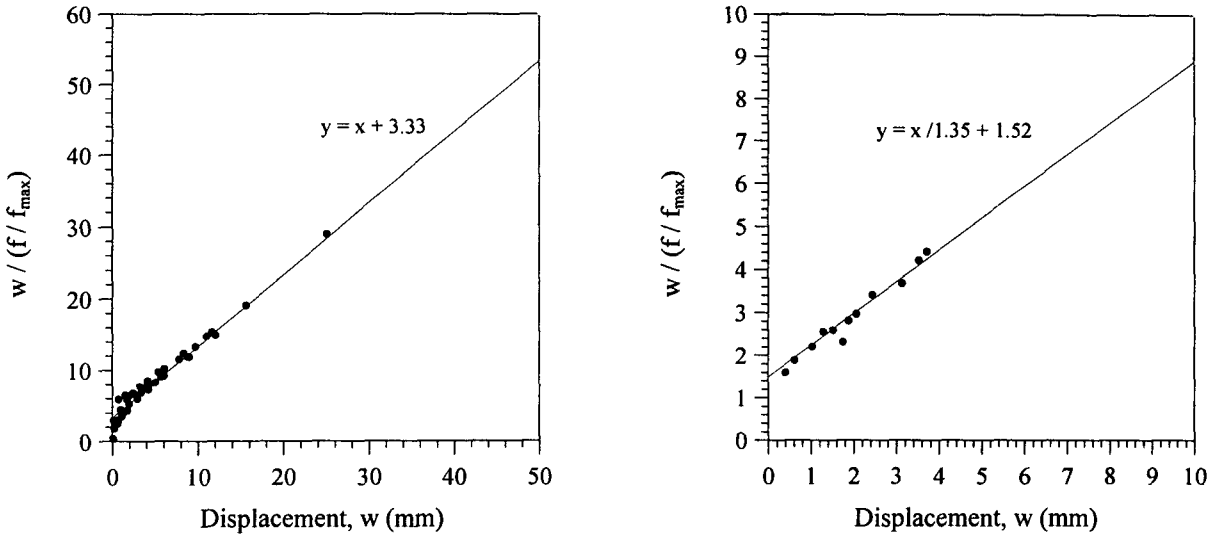

FIG. 9. Shear Load Transfer Curves in Transformed Coordinate: (a) Rough Surface; (b) Smooth Surface

Table 2 shows the values of the C factor and curve fitting constant, α_1 for highly weathered rocks based on the linear regression analysis. Finally, a single-modified hyperbolic shear transfer function of drilled shafts in highly weathered rocks can be obtained by substituting C and α_1 into equation (12).

Table 2. C and α_1 Parameters for Weathered Rocks

Surface Roughness	C Factor	Curve-Fitting Constant α_1
Rough	3.86	1.0
Smooth	6.26	1.35

8. COMPARISON WITH OTHER CASE HISTORIES

The present method is based on the modified load transfer model with soil coupling and shear load transfer function for weathered rocks. The validity of the proposed model was tested by comparing the results from the present approach with some of the measured results in detail in the following section.

8.1 Singapore Case

The load transfer characteristics of three instrumented drilled piers, numbered as M1, J1 and J2, installed in the weathered rocks of the Jurong Formation for actual construction projects in Singapore (Chang and Wong 1987) were

compared with the predicted values by the nonlinear load transfer analysis. Fig. 10 shows an idealization of the subsurface profile and shaft embedments for test piles: the test pile M1, 900 mm in diameter and 24 meters in length, test piles J1 and J2, both 1000 mm in diameter and 14 meters and 28 meters in lengths, respectively. The soil properties and shear transfer functions were chosen to represent a soil and rock based on soil borings and pile load tests. Table 3 shows the transfer functions (Baquelin's bi-linear, Castelli's hyperbolic) and material properties used in this study.

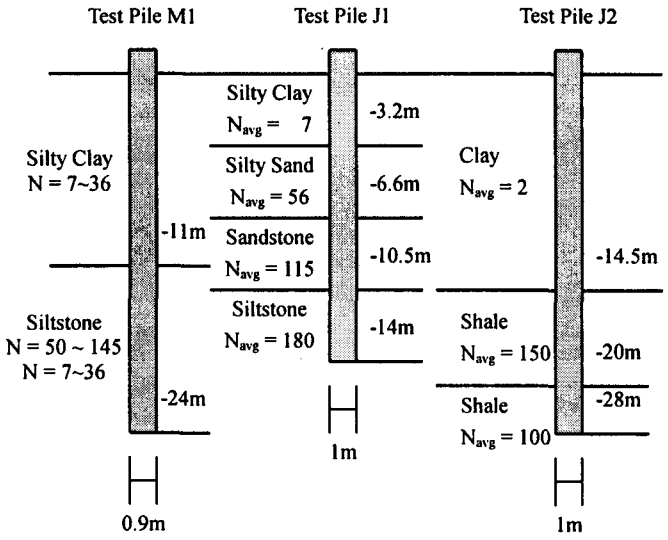

FIG. 10. Subsurface Profile and Shaft Embedments for Test Piles (Singapore Case)

Table 3. Subsurface Profile and Material Properties (Singapore Case)

Test Pile No.	Subsurface Profile		Transfer Function	Material Properties			Embedded Length in Rock (m)
	Soil Type	Depth		f_{max} (kN/m^2)	E_s (kN/m^2)	w_{max} (mm)	
M1	Silty Clay	0 ~ 11m	Bi-linear	25	-	1.0	13.0
	Siltstone	> 11m	Hyperbolic	400	1000000	-	
J1	Silty Clay	0 ~ 3.2m	Bi-linear	20	-	1.0	7.4
	Silty Sand	3.2 ~ 6.6m	Bi-linear	300	-	5.0	
	Sandstone	6.6 ~ 10.5m	Hyperbolic	150	400000	-	
	Siltstone	> 10.5m	Hyperbolic	400	1000000	-	
J2	Clay	0 ~ 14.5m	Bi-linear	30	-	1.0	13.5
	Shale	14.5 ~ 20m	Hyperbolic	400	3000000	-	
	Shale	> 20m	Hyperbolic	400	2000000	-	

Fig. 11 shows the predicted and observed load-settlement curves for test piles. The proposed method accurately predicts the general trend of the measured axial load when compared with the result from existing analysis : a reasonably good agreement between the present solution and the solution presented by the existing method was

obtained to predict the observed ones for the working load level (about 3,000 kN), beyond which the analysis by the existing method has a considerably smaller settlement when compared to the results by the present solution. This clearly demonstrates that for test piles there exists soil coupling, which is represented by s_2 (equation 1), so that this set of prediction results provide the influence of pile point settlement due to the transfer of shaft shear loading, especially as the structural load is increased to the ultimate limit state.

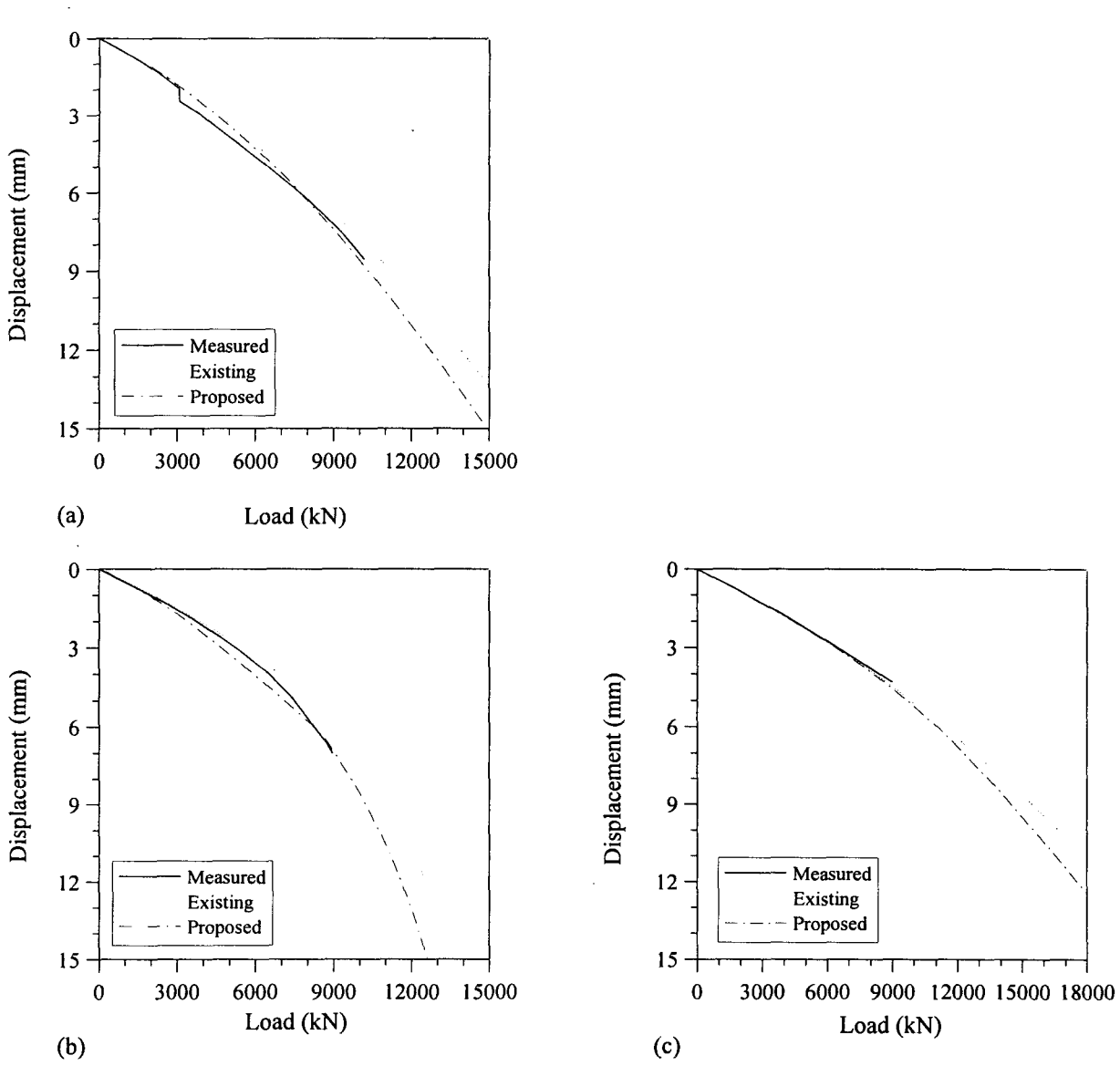

FIG. 11. Load-Displacement Curves at Pile Head (Singapore Case): (a) Pile M1; (b) Pile J1; (c)Pile J2

Fig. 12 shows the predicted and observed load transfer characteristics of test piles. The analysis by present approach based on the soil coupling effect approaches at most points closely to the measured value when compared to the results by the existing solution. This is because the existing method also ignores point displacement due to shaft shear transfer load and thus overestimates the point load transfer and smaller displacement in pile head movement.

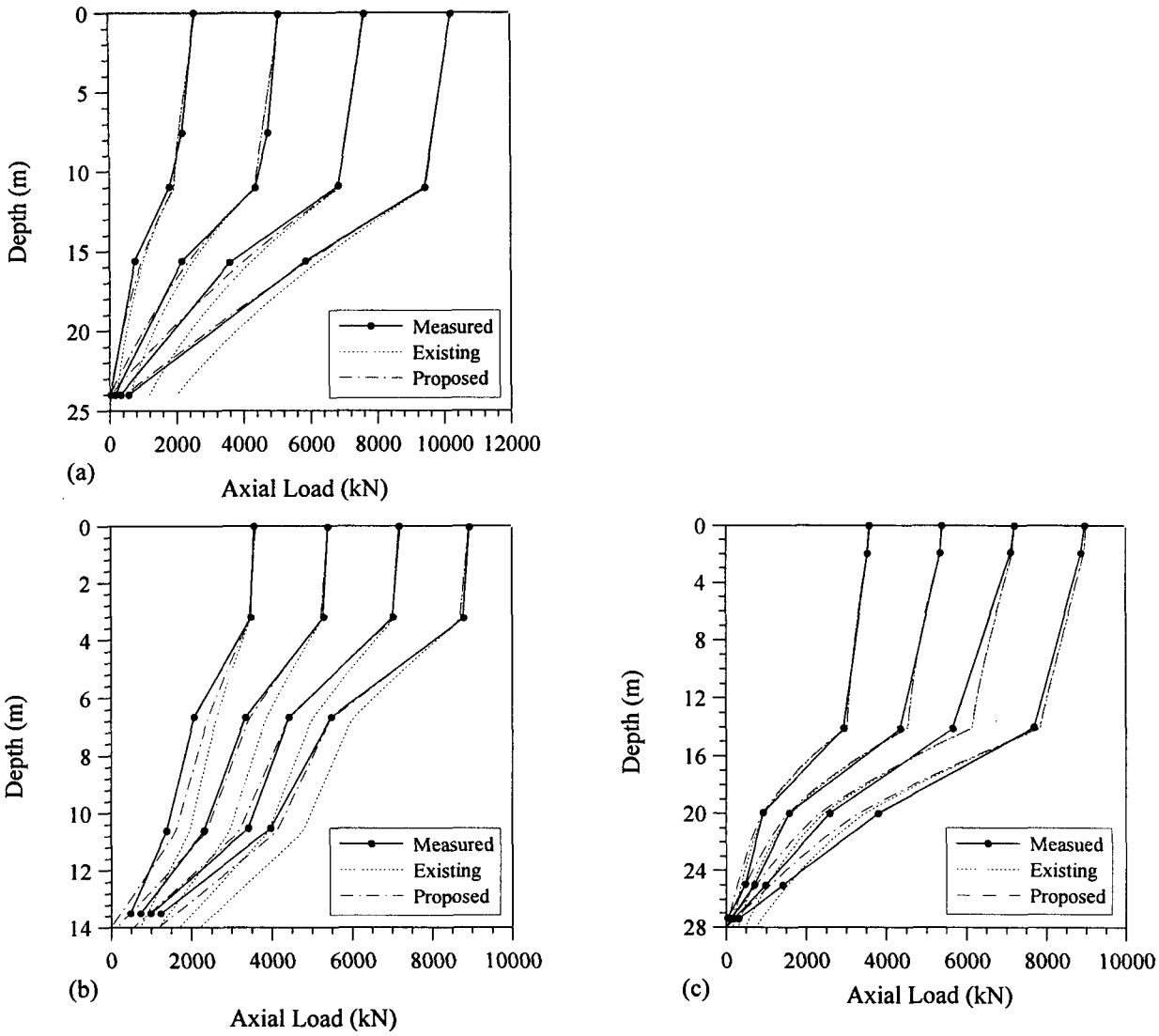

FIG. 12. Axial Load Distributions (Singapore Case): (a) Pile M1; (b) Pile J1; (c) Pile J2

8.2 Seohae Case

The load transfer characteristics of three instrumented drilled shafts, numbered as SN1, SN2 and ST1, installed in the weathered rocks of the Seohae Bridge pier foundation were compared with the predicted values by the present approach. Fig. 13 shows an idealization of the subsurface profile and shaft embedments for test piles: the test piles SN1, SN2 and ST1 are all 1500 mm in diameter and 32.7 meters, and 11.3 meters and 18.2 meters in lengths, respectively. After installation of the piles, the pile load tests were performed for the purpose of identifying the bearing capacity and thus no information was available on the load transfer distribution in the test piles. The soil properties and shear transfer functions were chosen to represent a soil and weathered rock based on site investigation and pile load tests. Table 4 shows the transfer functions (Baquelin's bi-linear, Castelli's hyperbolic, modified hyperbolic) and material properties used in this study.

Fig. 14 shows the predicted and observed load-settlement curves for the test piles. The proposed method predicts well the general trend of the measured axial load when compared with the result by existing analysis. Reasonably good agreement between the present solution and the solution presented by the existing method was obtained for the working load level, beyond which the analysis by the existing method has a considerably smaller settlement than the settlement calculated by the present solution. It is important to mention that a definite s_2 effect, inspite of a test pile, SN2 embedded into shallow depth, was observed in case of relatively small stiffness of bearing layer, as opposed to the Oklahoma case. This clearly demonstrates that for test piles there exist soil coupling, which is represented by s_2 (equation 1), so that this set of prediction results provide the influence of pile point settlement due to transfer of shaft shear loading as structural load is increased to ultimate limit state.

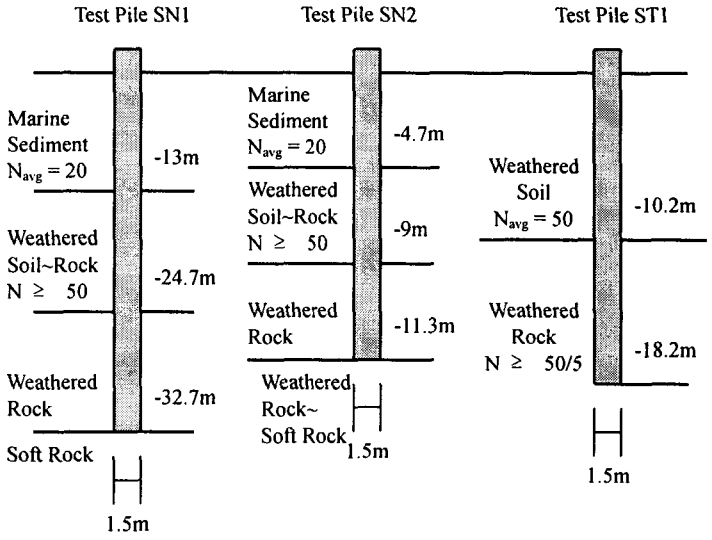

FIG. 13. Subsurface Profile and Shaft Embedments for Test Piles (Seohae Case)

Table 4. Subsurface Profile and Material Properties (Seohae Case)

Test Pile No.	Subsurface Profile		Transfer Function	Material Properties			Embedded Length in Rock (m)
	Soil Type	Depth		F_{max} (kN/m^2)	E_s (kN/m^2)	w_{max} (mm)	
SN1	Marine Sediment	0 ~ 13.0m	Bi-linear	40	-	1.0	19.7
	Weathered Soil ~ Weathered Rock	13.0 ~ 24.7m	Vijayvergiya	300	-	5.0	
	Weathered Rock	24.7 ~ 32.7m	Modified Hyperbolic	800	300000	-	
	Soft Rock	> 32.7m	Hyperbolic	-	3000000	-	
SN2	Marine Sediment	0 ~ 4.7m	Bi-linear	40	-	1.0	6.6
	Weathered Soil ~ Weathered Rock	4.7 ~ 9.0m	Vijayvergiya	300	-	5.0	
	Weathered Rock	9.0 ~ 11.3m	Modified Hyperbolic	800	300000	-	
	Weathered Rock ~ Soft Rock	> 11.3m	Hyperbolic	-	1000000	-	
ST1	Weathered Soil	0 ~ 10.2m	Vijayvergiya	50	-	10.0	8.0
	Weathered Rock	> 10.2m	Modified Hyperbolic	800	300000	-	

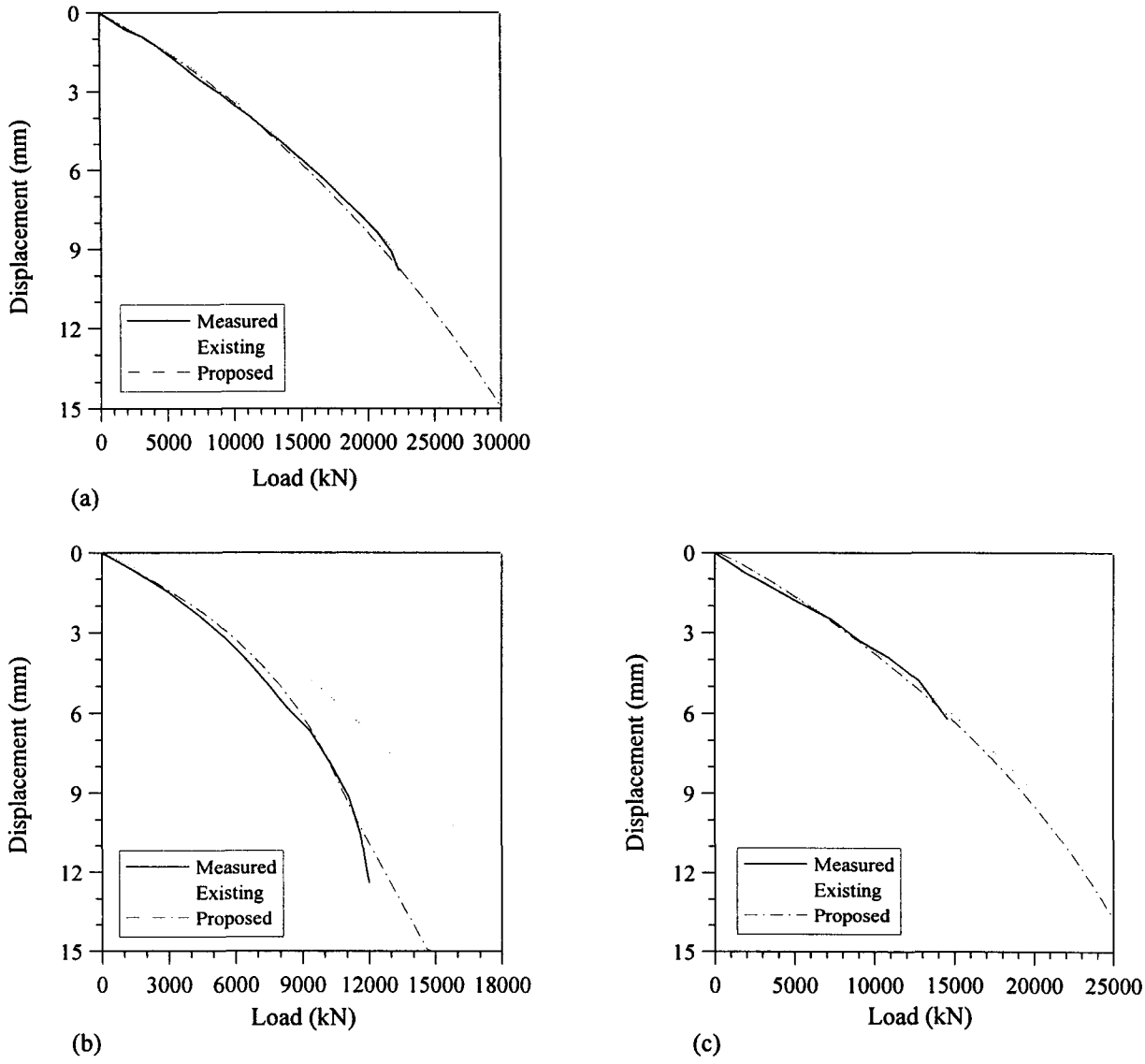

FIG. 14. Load-Displacement Curves at Pile Head (Seohae Case): (a) Pile SN1; (b) Pile SN2; (c) Pile ST1

9. CONCLUSION

The main objective of the analysis described herein was to investigate the load distribution and deformation of drilled shafts installed in highly weathered rock using an analytical study and field load tests. A limited study of the response of drilled shafts was performed to examine the soil coupling effect for pile length, load-carrying capacity and two different transfer functions. When applied to drilled shafts installed in the weathered rocks, the parametric studies have clearly demonstrated the important interaction effect of drilled shafts subjected to axial forces. From the findings of this study, the following conclusions are drawn:

1. By taking into account the soil coupling effect, the shear transfer function of a single-modified hyperbolic model is appropriate and realistic to represent a pile-soil interaction for drilled shafts in weathered rocks.
2. The fitness of initial tangent modulus, S_i is more closely related to $E_s = \sqrt{D}$ than to E_s / D. Therefore, commonly used methods for calculating initial tangent modulus by using the results of E_s / D values can substantially

underestimate the degree of initial slope, S_i, in realistic situations.

3. Coupling effect is generally more significant for long piles than for short piles and the analysis by the present method has considerably larger settlement when compared to the results by existing methods. However, even in short friction piles embedded in shallow depth, there is a definite coupling effect with small stiffness of bearing layer relative to the surrounding layers. Thus, using the modified transfer function would be safe situation in the design of drilled shafts based on the concept of serviceability limit state.

10. REFERENCES

Baquelin, F., Frand, R., and Jezequel, J. F. (1982). "Parameters for Friction Piles in Marine Soils" *2nd International Conf. in Numerical Methods for Offshore Piling,* Austin.

Chang, M. F. and Wong, I. H. (1987). "Shaft Friction of Drilled Piers in Weathered Rock" *Proceedings of 6th International Conference on Rock Mechanics*, Montreal, ISRM, 313-318.

Deere, D. V. (1968). "Geological Considerations *Rock Mechanics in Engineering Practice"*, Ed. by Stagg K. G. and Zienkiewicz O. C., Wiley, 1-20.

De Beer, E. (1986). "Different Behavior of Bored and Driven Piles" *Proceedings of 6th Danubian Conference on Soil Mechanics and Foundation Engineering*, Budapest, 307-318.

Engeling, D. E. and Reese, L. C. (1974). "Behavior of Three Instrumented Drilled Shafts under Short Term Axial Loading" *Research Report 176-3*, Center for Highway Research, The University of Texas at Austin.

Ghionna, V. N. (1993). "Base Capacity of Bored Piles in Sands from In-situ Tests" *Proceedings of 2nd International Geotechnical Seminar on Deep Foundation on Bored and Auger Piles*, Ghent.

Goeke, P. M. and Hustad, P. A. (1979). "Instrumented Drilled Shafts in Clay-Shale" *Proceedings of Symposium on Deep Foundations*, Georgia, ASCE, 149-165.

Goodman, R. E. (1980). *Introduction to Rock Mechanics.* John Wiley and Sons, New York, 317-325.

Horvath, R. G., Kenney, T. C., and Kozicki, P. (1983). "Methods of Improving the Performance of Drilled Piers in Weak Rock" *Canadian Geotechnical Journal,* Vol. 20, 758-772.

Johnston. I. W. (1994). "Movement of Foundations on Rock" *Geotechnical Special Publication No. 40, Vertical and Horizontal Deformations of Foundations and Embankments,* Vol. 2, 1703-1717.

Lee, S. G. and de Freitas, M. H. (1989). "A Revision of the Description and Classification of Weathered Granite and Its Application to Granites in Korea" *Journal of Engineering Geology, 22*(1), 31-48.

Mattes, N. S. and Poulos, H. G. (1969). "Settlement of Single Compressible Pile" *Journal of Soil Mechanics and Foundation Division*, ASCE, 95(1), 189-207.

O'Neill, M. W. and Hassan, K. M. (1994). "Drilled Shafts : Effects of Construction on Performance and Design Criteria" *Proceedings of International Conference on Design and Construction of Deep Foundations*, Vol.1, FHWA, Orlando, 137-187.

Poulos, H. G. and Davis, E. H. (1968). "The Settlement Behaviour of Single Axially Loaded Incompressible Piles and Piers" *Geotechnique*, Vol. 18, 351-371.

Poulos, H. G. and Mattes, N. S. (1969). "The Behaviour of Axially Loaded End-Bearing Piles" *Geotechnique*, Vol. 19, 285-300.

Reese, L. C. and O'Neill, M. W. (1988). "Drilled Shafts : Construction Procedures and Design Methods" *Publication No. FHWA-HI-88-042*, Federal Highway Administration, Washington.

Townsend, F. C., Dunkelberger, C. E., and Bloomquist, D. (1993). "Drilled Shaft Friction Evaluation via Pullout Tests" *Geotechnical Special Publication No. 38, Design and Performance of Deep Foundations : Piles and Piers in Soil and Soft Rock* Ed. by Nelson P. P., Smith T. D. and Clukey E. C., ASCE, 64-75.

Vijayvergiya, V. N. (1997). "Load-Movement Characteristics of Piles" *4th Annual Symposium of the Waterway, Port, Coastal and Ocean Division of ASCE,* Long Beach.

Table 1. Material Properties and Geometries

Surface Roughness		Rough	Smooth
Soil Properties	Internal Friction Angle ϕ' (°)	38	32
	Cohesion, c' (kN/m^2)	300	600
	Dilation Angle, ψ (°)	2	0
	Elastic Modulus, E_s (kN/m^2)	100000, 300000, 600000, 900000, 1200000, 1500000, 1800000, 2000000	
	Poisson's Ratio, v	0.30	
	Unit Weight, γ (kN/m^3)	21.0	
Pile Properties	Elastic Modulus, E_s (kN/m^2)	35000000	
	Poisson's Ratio, v	0.17	
	Length, L (m)	1.0	
	Diameter, D (mm)	165, 300, 600, 900, 1200, 1500	

Table 2. C and α_1 Parameters for Weathered Rocks

Surface Roughness	C Factor	Curve-Fitting Constant α_1
Rough	3.86	1.0
Smooth	6.26	1.35

Table 3. Subsurface Profile and Material Properties (Singapore Case)

Test Pile No.	Subsurface Profile		Transfer Function	Material Properties			Embedded Length in Rock (m)
	Soil Type	Depth		f_{max} (kN/m^2)	E_s (kN/m^2)	w_{max} (mm)	
M1	Silty Clay	0 ~ 11m	Bi-linear	25	-	1.0	13.0
	Siltstone	> 11m	Hyperbolic	400	1000000	-	
J1	Silty Clay	0 ~ 3.2m	Bi-linear	20	-	1.0	7.4
	Silty Sand	3.2 ~ 6.6m	Bi-linear	300	-	5.0	
	Sandstone	6.6 ~ 10.5m	Hyperbolic	150	400000	-	
	Siltstone	> 10.5m	Hyperbolic	400	1000000	-	
J2	Clay	0 ~ 14.5m	Bi-linear	30	-	1.0	13.5
	Shale	14.5 ~ 20m	Hyperbolic	400	3000000	-	
	Shale	> 20m	Hyperbolic	400	2000000	-	

Table 4. Subsurface Profile and Material Properties (Oklahoma Case)

Test Pile No.	Subsurface Profile		Transfer Function	Material Properties		Embedded Length in Rock (m)
	Soil Type	Depth		f_{max} (kN/m^2)	E_s (kN/m^2)	
S1	Shale	3.4 ~ 11.1m	Hyperbolic	420	1000000	3.0
	Shale & Limestone	> 11.1m	Hyperbolic	-	2000000	
S2	Shale	3.4 ~ 11.1m	Hyperbolic	370	500000	5.3
	Shale & Limestone	> 11.1m	Hyperbolic	-	2000000	

Table 5. Subsurface Profile and Material Properties (Seohae Case)

Test Pile No.	Subsurface Profile		Transfer Function	Material Properties			Embedded Length in Rock (m)
	Soil Type	Depth		F_{max} (kN/m^2)	E_s (kN/m^2)	w_{max} (mm)	
SN1	Marine Sediment	0 ~ 13.0m	Bi-linear	40	-	1.0	19.7
	Weathered Soil ~ Weathered Rock	13.0 ~ 24.7m	Vijayvergiya	300	-	5.0	
	Weathered Rock	24.7 ~ 32.7m	Modified Hyperbolic	800	300000	-	
	Soft Rock	> 32.7m	Hyperbolic	-	3000000	-	
SN2	Marine Sediment	0 ~ 4.7m	Bi-linear	40	-	1.0	6.6
	Weathered Soil ~ Weathered Rock	4.7 ~ 9.0m	Vijayvergiya	300	-	5.0	
	Weathered Rock	9.0 ~ 11.3m	Modified Hyperbolic	800	300000	-	
	Weathered Rock ~ Soft Rock	> 11.3m	Hyperbolic	-	1000000	-	
ST1	Weathered Soil	0 ~ 10.2m	Vijayvergiya	50	-	10.0	8.0
	Weathered Rock	> 10.2m	Modified Hyperbolic	800	300000	-	